

Direct numerical simulations of homogeneous isotropic turbulence in a dense gas

A Giaque¹, C Corre¹ and M Menghetti¹

¹ LMFA - Laboratoire de Mecanique des Fluides et d'Acoustique

Ecole Centrale de Lyon, 36 avenue Guy de Collongue, 69134 Ecully Cedex, France

E-mail: alexis.giaque@ec-lyon.fr

Abstract. A study of turbulence in BZT dense gas flows is performed using DNS. It is shown that for a large but realistic intensity, the turbulence in dense gas flows behaves in a highly compressible manner when the average thermodynamic state lies within the inversion region in which the gas fundamental derivative is negative. A close similarity is observed in the evolution of the kinetic energy when the initial turbulent Mach number and the Taylor Reynolds number are matched regardless of the Equation of State (EoS) considered. A large turbulent Mach number is yet more easily attained in dense gas flows lying in the inversion region because of the low speed of sound associated with it. In this case the turbulence shows a highly compressible evolution with periodic exchanges between the internal and kinetic energies. In order to assess the capabilities of currently available Large Eddy Simulation (LES) subgrid-scale models, a-posteriori tests are performed using the dynamic Smagorinsky model. Coherently with the hypothesis it relies on, the model perfectly captures the evolution of the kinetic energy when the turbulent Mach number is low enough. When using the perfect gas EoS at a higher turbulent Mach number the agreement is reasonable. Yet, when the average thermodynamic state lies within the inversion region and when using the thermal and caloric Martin&Hou EoS, the model is not able to capture the correct evolution of the kinetic energy. The results presented in this study call for a specific research effort directed towards the assessment and possibly the development of advanced subgrid-scale models for LES of turbulent dense gas flows.

1. Introduction

Engineering systems harvesting dense gas thermodynamic cycles for the recovery of fatal heat (i.e. heat that is lost in the output gases during any transformation process) experience an accelerated development under the combined effect of the increase of the energy price and of the public awareness for climate issues. Companies developing this technology face numerous challenges among which some come from a lack of basic knowledge regarding the turbulent flows of dense gases in expanders. Indeed, to obtain efficient turbomachinery systems, numerous prototypes are designed on the basis of Computational Fluid Dynamics (CFD) predictions before being tested. Today, Reynolds Averaged Navier-Stokes (RANS) simulations have become a usual tool in the design stage of these machines. Large Eddy Simulation (LES) is an additional useful tool for the understanding of intrinsically unsteady phenomena occurring in Organic Rankine Cycle (ORC) turbines. Yet, for both these methods, the turbulence models upon which they rely were all developed in the context of perfect gases.

Among dense gases, Bethe-Zel'dovitch-Thompson (BZT) fluids [1] have raised a particular interest because their fundamental derivative defined as $\Gamma = 1 + \frac{\rho}{a} \left[\frac{\partial a}{\partial \rho} \right]_s$, where ρ is the density



and a the speed of sound, can be lower than one and even become negative in which case shock waves are dampened along with the associated losses. It is also expected that for appropriate inflow conditions, the turbulent Mach number will be large enough to modify the behavior of turbulence down to the smallest scales, which will significantly impact viscous losses. In order to assess the need for accurate and reliable models tailored for dense gases, it is first necessary to study turbulence in dense gas flows without resorting to a turbulence model. In this study, Direct Numerical Simulation (DNS) is used to investigate decaying homogeneous isotropic turbulence (HIT) and understand the influence of thermodynamics on turbulence in dense gas flows. The article is organized as follows. In the first section, the numerical tool used to perform DNS is introduced along with the test cases performed in the study to compare perfect and dense gas behavior. Section 2 focuses on the DNS results and compares the properties of turbulence between the different test cases. Section 3 presents, for the different test cases, a comparison between results obtained by LES using the dynamic Smagorinsky model and DNS.

2. Numerical Setup and Test cases

For this study, FC-70 is used as the working fluid. FC-70 is suspected to be dense enough to possess an inversion region in which its fundamental derivative is negative [2]. All along this study, the initial pressure, temperature and specific volume correspond to the thermodynamic state 4 for the first MAH case in the article of Fergason *et al* [3] in which the reduced (normalized by the critical values) pressure and specific volume are respectively equal to 0.9866 and 1.5733. All decaying HIT cases proposed in this study are performed for an initial Taylor Reynolds number equal to 75 and simulations are initiated using an incompressible homogeneous isotropic turbulent velocity field following the Passot-Pouquet spectrum with k_e the wavelength of maximum initial kinetic energy defined by the relationship $Re_\lambda = 2u_{rms}/(\nu k_e)$. Given the low speed of sound obtained using the thermal and caloric Martin&Hou [4] Equation of State (EoS) for the chosen thermodynamic point, a 20 m/s turbulent velocity translates into a turbulent Mach number equal to 0.8. This case, referred to as case MAH1 from now on, is the main physical case of interest in the present study. In order to assess the influence of the average thermodynamic state, an additional test case is performed using the Martin&Hou EoS for the same turbulent velocity and Taylor Reynolds number but for a lower reduced pressure equal to 0.1. In this thermodynamic region much further away from the saturation curve, the speed of sound is larger and this translates into a smaller turbulent Mach number equal in this case to 0.3. This test case will be referred to as MAH2. Additionally, in order to assess the influence of the EoS, two cases using the perfect gas EoS are performed in which for the first one, the turbulent velocity is the same as for MAH1 and for the second one the turbulent Mach number is the same as for MAH1. These cases will be referred to respectively as PG1 and PG2. For cases MAH1 and MAH2, the Equation of state is the one proposed by Martin and Hou [4]. For these cases, the dynamic viscosity as well as the thermal conductivity follow the model proposed by Chung *et al* [5]. For cases PG1 and PG2, the dynamic viscosity follows Sutherland's law and a constant Prandtl number equal to 0.71 is used. Table 1 summarizes the characteristics of each of the test cases performed in this study. Note that even if the reduced pressure and temperature are close to unity for both PG1 and PG2 cases, it does not influence the results since the Perfect Gas EoS is used.

DNS are performed using the numerical solver AVBP [6]. The parallel LES and DNS code solves the full compressible Navier-Stokes equations using a two-step time-explicit Taylor-Galerkin scheme (TTGC or TTG4A) for the hyperbolic terms based on a cell-vertex formulation [7]. The schemes provide high spectral resolution as well as low numerical dissipation and dispersion. They also ensure third-order accuracy in space and third-order (TTGC) or

Table 1. Physical characteristics of the DNS test cases

| Case name | Turbulent velocity (m/s) | Turbulent Mach Number | Reduced Pressure | Reduced Temperature |
|-----------|--------------------------|-----------------------|------------------|---------------------|
| MAH1 | 20 | 0.8 | 0.98 | 1.0015 |
| MAH2 | 20 | 0.3 | 0.1 | 1.0015 |
| PG1 | 20 | 0.32 | 0.98 | 1.0015 |
| PG2 | 63 | 0.8 | 0.98 | 1.0015 |

fourth-order (TTG4A) accuracy in time [7]. The main difference between TTGC and TTGA4 is linked to the amplification factors of the schemes that show a different behavior on small spatial wave length structures: TTG4A has a more dissipative behavior on small wave lengths compared to TTGC. Nevertheless, TTG4A is less prone to numerical instabilities issued by the centered spatial discretization. These schemes have been extensively validated in the context of Large Eddy Simulation [8, 9, 10] but their precision can be thought of as being in the low limit for performing Decaying HIT Direct Numerical Simulations (DNS). In order to make sure the results are reliable, for each case three simulations are performed using different spatial resolutions. The first computation uses 240^3 cells, the second one 320^3 and the most resolved 400^3 . Given the common initial Taylor Reynolds number, the respective resolutions correspond to discretizations of the Kolmogorov length scale with 2, 2.5 and 3 points respectively. Figure 1 displays the temporal evolution of the kinetic energy and enstrophy. The kinetic energy is normalized by its initial value, the enstrophy is normalized by the maximum value reached in the most resolved case and the time is normalized by the characteristic turn-over time which is defined as $\tau_0 = L_i/u_{rms}$ and depends on the case considered. Figure 1 shows that all computations provide exactly the same evolution both for the kinetic energy and for the enstrophy although this last quantity is of a higher order. This result is coherent with the fact that in order to provide that evolution, the Kolmogorov length scale does not need to be perfectly discretized given the fact that only a very small percentage of the kinetic energy remains at this scale [11].

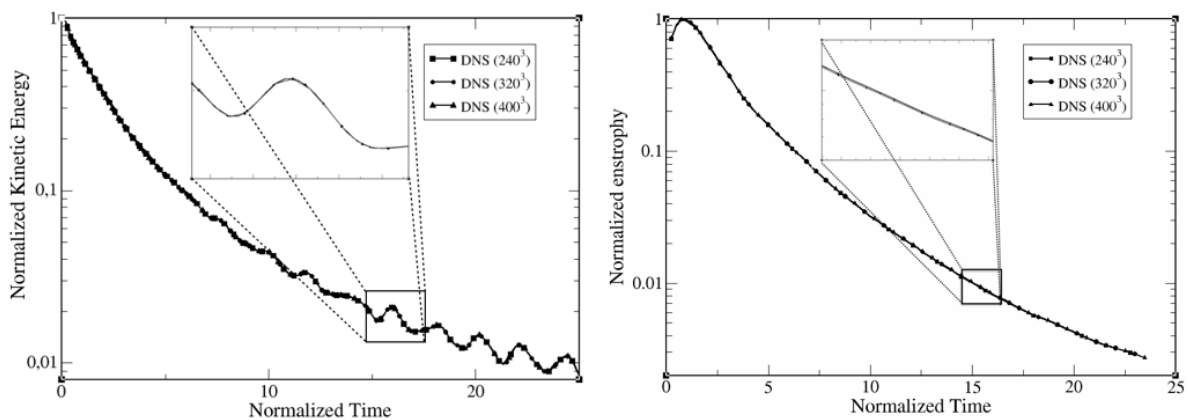


Figure 1. Evolution of the normalized kinetic energy (left) and normalized enstrophy (right) with time in the MAH1 case for three different spatial resolutions (240^3 , 320^3 and 400^3).

3. Results

3.1. Kinetic Energy and Skewness

The cases corresponding to large initial turbulent Mach number show a transition period before they adapt to the initial incompressible condition as already described in [12, 13]. During this period, shocklets appear in cases MAH1 and PG2. Figure 2 compares the dilatation between the two cases. One can see that because the average thermodynamic state lies within the inversion region for the MAH1 case, regions of very large dilatation are present together with compression shocklets. In the PG2 case, only compression shocklets are visible. This result is coherent with recent findings from Sciacovelli & Cinnella [14].

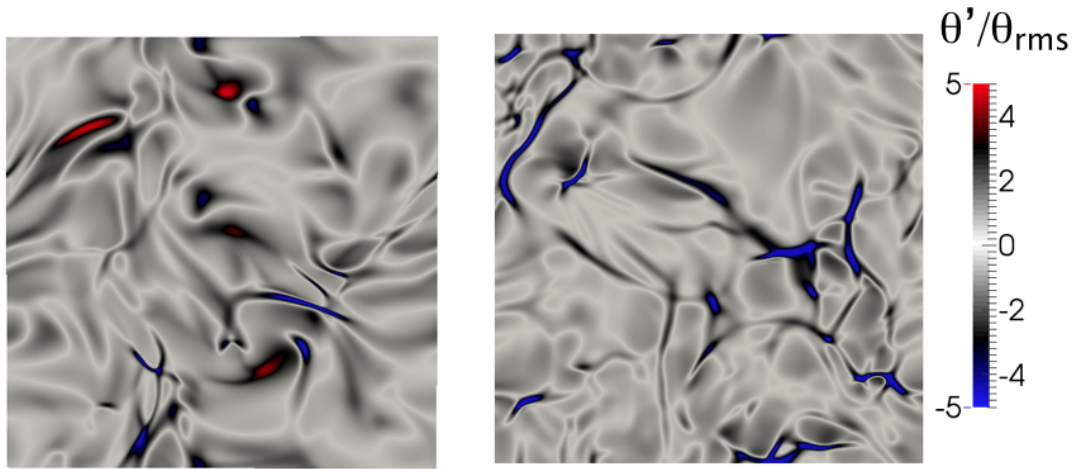


Figure 2. Sectional cut of the flow colored by the local divergence divided by its spatial r-m-s value at time $\tau = 1$. Left:MAH1, Right:PG2.

Figure 3 compares for the four cases of table 1 the evolution of the kinetic energy with respect to time. The first remark that can be made is that the temporal evolution of the kinetic energy depends more on the common value of the turbulent Mach number than on the type of EoS given the fact that the Taylor Reynolds number is identical for all cases. Indeed, cases MAH2 and PG1 show almost identical evolutions of their kinetic energy. In cases MAH1 and PG2, the evolutions are rather similar until $t/\tau = 15$, with a slightly smaller slope afterwards for MAH1. An important aspect for cases MAH1 and PG2 is the observed oscillation of the kinetic energy starting around $t/\tau = 8$ for both cases. This has already been observed by Kida & Orszag [12] and is related to a periodic exchange between the internal and kinetic energies through the pressure gradient term.

Also of interest is the evolution of the skewness of the velocity gradient as this quantity is expected to be statistically constant in decaying HIT. Figure 4 compares the evolution of this statistical quantity in the cases using the Martin&Hou EoS. One can see on the left that in the case MAH2, the isotropy is well preserved and that skewness factors closely match the value of -0.4 experimentally obtained and also predicted by the Heisenberg's transfer theory [15, 16]. In cases MAH1 and PG2, the use of the Passot-Pouquet spectrum, derived from incompressible turbulence studies, induces an adaptation period during which the skewness rapidly evolves.

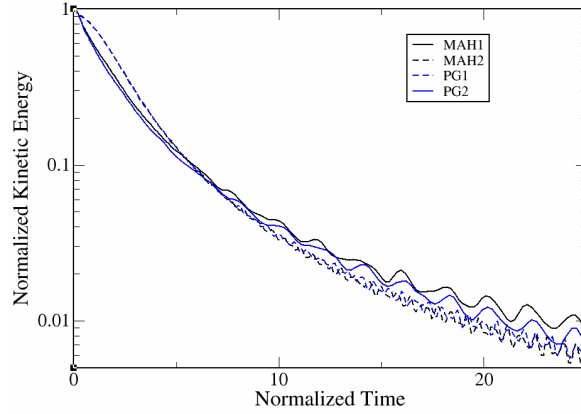


Figure 3. Evolution of the normalized kinetic energy with time.

Once the numerical computation has adapted to the initial solution, the values tend to remain close to the theoretical value of -0.4. One can also note that for $t/\tau > 8$, some departure from isotropy occurs as the three directional skewness factors do not perfectly follow the same temporal evolution. Although no definitive proof is provided here, it is reasonable to assume that this behavior is linked with the observed periodic exchange between the internal and kinetic energies shown in Fig 3, that starts at the same instant in time for case MAH1. Similar results are obtained for cases PG1 and PG2. Regardless of the case considered, it is interesting to note that some stationarity is achieved for this statistical quantity. Together with the already demonstrated grid convergence, it enables the analysis and comparisons of Turbulent Kinetic Energy (TKE) spectra with a fair degree of confidence.

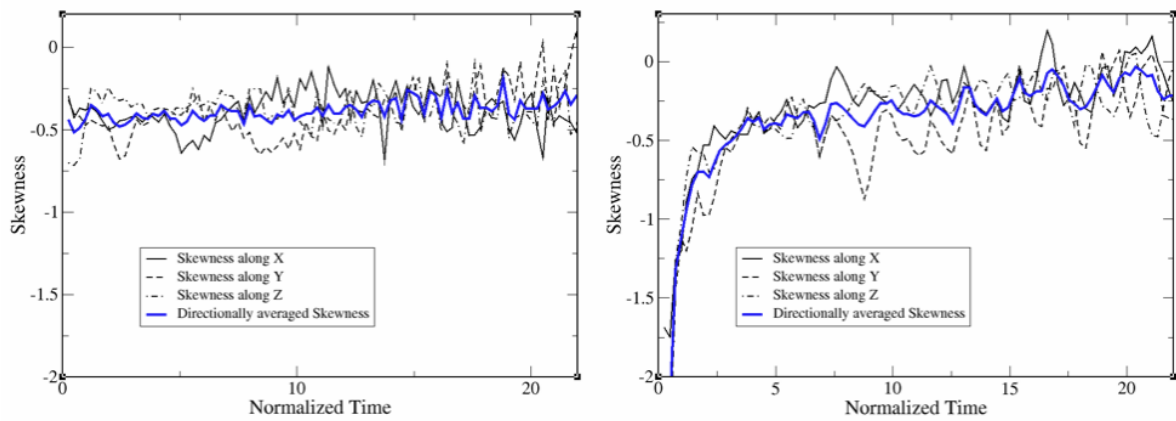


Figure 4. Evolution of the skewness of the velocity gradient with time. Left:MAH2, Right:MAH1

3.2. Spectrum and Thermodynamics

The temporal evolution of the spectra of normalized TKE (i.e $\widehat{E}_n = (\widehat{E}_c/\rho) * \epsilon^{-2/3} k^{5/3}$) is first analyzed for cases PG1 and MAH2. In these cases, the low initial turbulent Mach number

leads to an almost incompressible evolution of the turbulence. Therefore, as verified in Figure 5 the non-dimensionalization provides spectra that collapse on each other at all times. Because of the low Taylor Reynolds number used in this study the inertial region of the spectrum is quite narrow. In this region, the retrieved constant is equal to 1.2 which is smaller than the Kolmogorov constant ($\approx 1.5 - 1.6$). From this comparison, one can note that at low turbulent Mach number FC-70, though being a highly compressible fluid, behaves in an incompressible manner as far as turbulence is concerned. This behavior goes together with a monotonic decrease of the kinetic energy as observed in Fig 3.

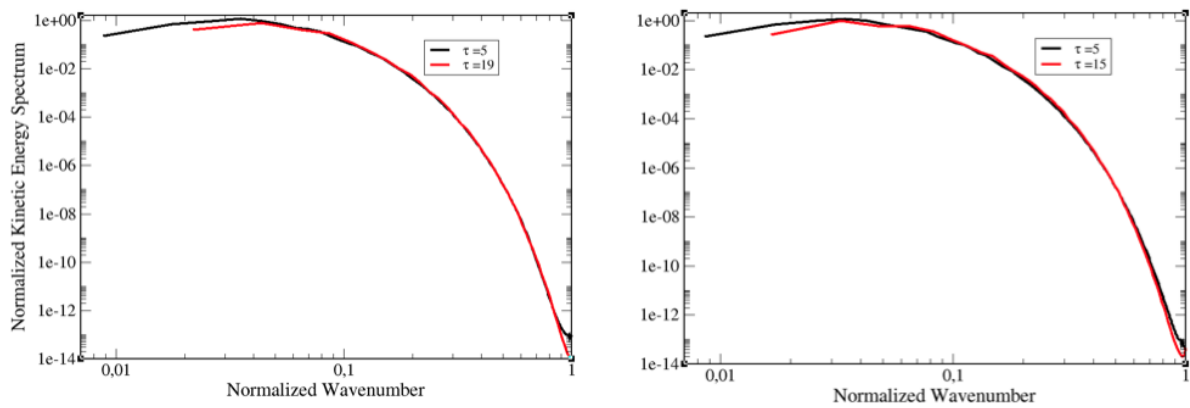


Figure 5. Normalized spectrum of TKE at different instants in time for the case MAH2 (left) and PG1 (right).

Cases MAH1 and PG2 are much more challenging in terms of physical interpretation. Figure 6 presents a comparison of the temporal evolution of the normalized TKE spectra for the two cases. First, one can observe that the overall levels are quite different between MAH1 and PG2. The PG2 case shows a much more energetic content at small scales. For example, the non dimensional TKE level of 10^{-4} is reached by structures only 1.5 times larger than the Kolmogorov length whereas such levels in the MAH1 case correspond to turbulent structures two times larger. Comparing Figure 6 with Figure 5 results, it is interesting to see that as far as the overall TKE spectrum level is concerned, the MAH1 case is much closer to the MAH2 and PG1 cases than the PG2 case.

Another important observation can be made from analyzing Figure 6. For both MAH1 and PG2 cases, the normalized spectra do not collapse on each other for length scales smaller than approximately 5 Kolmogorov length scales. Depending on the time at which the normalized spectrum of TKE is observed, relative levels fluctuate in the region of small but yet well resolved length scales. Grid convergence analysis applied to the TKE spectra (not shown here for brevity reasons) clearly demonstrate that these fluctuations are not produced by some numerical dissipation issue but are most probably connected to physical phenomena taking place at these scales. Because this behavior occurs for the two cases also showing temporal oscillations of the kinetic energy (see Fig 3) one can reasonably suppose that there is a connection between the two features of the turbulence. Yet, the fact that the normalized spectra do not collapse over time in the region of small length-scales ($l < 5l_\eta$) also shows that an additional parameter should be considered during the nondimensionalization process in addition to the wavenumber k and the dissipation ϵ .

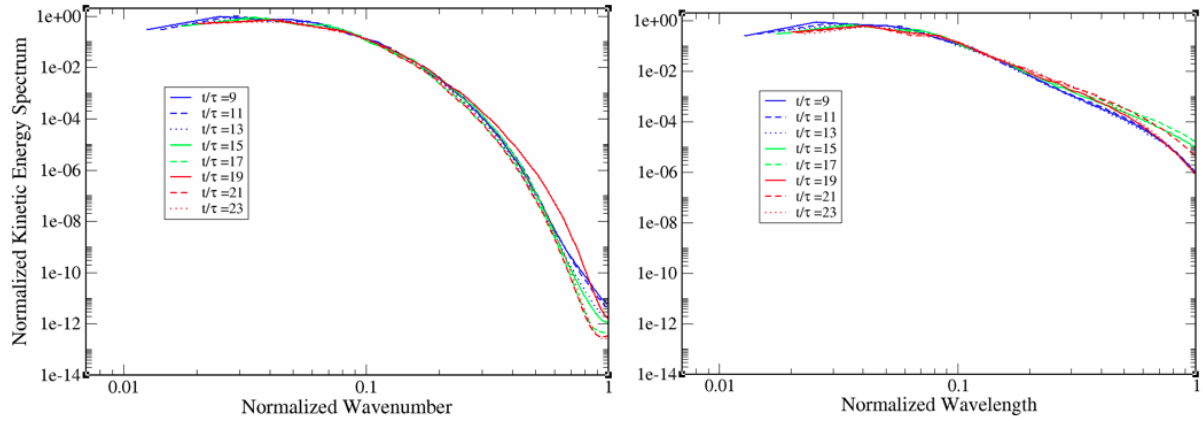


Figure 6. Normalized spectrum of TKE at different instants in time for the case MAH1 (left) and PG2 (right).

Also of interest for case MAH1 is the temporal evolution of the distribution of thermodynamic states. One can see in Figure 7 the evolution of the curves formed, at different reduced times in the simulation, by the maxima of the reduced pressure distribution for each reduced volume. Most represented thermodynamic states closely follow the adiabatic curve passing through the initial conditions. Because static thermodynamic conditions are of course influenced by the kinetic energy, they lie inside the inversion region but also cross the limit $\Gamma = 0$. For a large part of the total temporal extension of the simulation ($t/\tau < 30$) there is a coexistence of both types of thermodynamic conditions. Although it is not further analyzed here, it is interesting to note that such a distribution might include very close points in physical space being in highly different thermodynamic states, for instance one being in the inversion region and the other outside. In this case, judging from previous inviscid results obtained by Ferguson *et al* [3], one would expect to detect the presence of expansion shocklets as seemingly observed in Fig 2. Finally, as time goes by, the initially spread distribution slowly collapses back to the initial single mean thermodynamic point though with a slightly larger temperature corresponding to the dissipation of the entire kinetic energy into internal energy.

3.3. *A-posteriori Large eddy simulation*

The previous sections show that given a realistic intensity, the behavior of turbulence in dense gas flows is significantly modified by the thermodynamic state of the fluid. It is therefore interesting to assess the present capability of usual LES subgrid-scale models to capture the evolution of the kinetic energy in dense gas flows. To do so, the dynamic Smagorinsky model is used to simulate cases MAH1, MAH2, PG1 and PG2 with two different levels of spatial resolution. A first resolution corresponding to 32^3 elements is used. In this case, the grid spacing corresponds to 4 Kolmogorov length scales. This resolution, being already quite fine, leads to grid filtering lying in the dissipation range which is not representative of LES requirements. Therefore a second resolution is considered comprising 16^3 elements. For this last resolution, the grid spacing corresponds to 8 Kolmogorov length scales which although still not in the inertial range makes it more representative of LES requirements. Figure 8 shows that for cases MAH2 and PG1, LES is able to correctly capture the temporal evolution of the kinetic energy with a good accuracy. This confirms that when the turbulent Mach number is low enough, thermodynamics does not

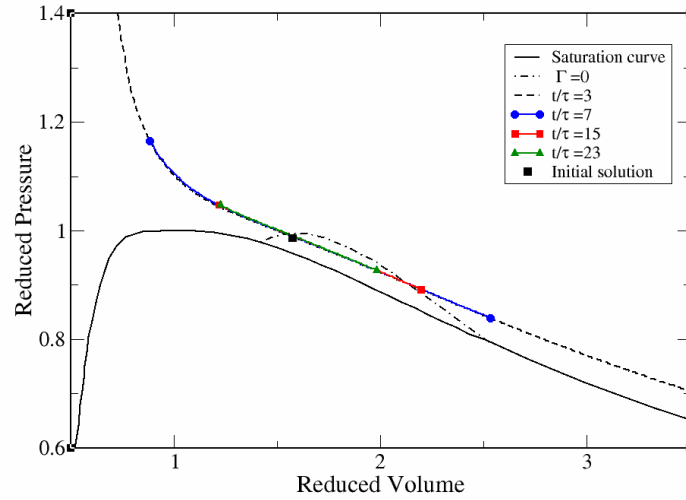


Figure 7. Distribution of the thermodynamic states in the $p_r - v_r$ diagram in the case MAH1 at different instants in time.

significantly influence turbulence. In these cases, the standard dynamic Smagorinsky subgrid-scale model is good enough to study turbulent dense gas flows using LES. For this condition to be verified though, the turbulent velocity needs to be small enough compared to the speed of sound. This is where the thermodynamic inversion region plays a key role. Indeed, when the average thermodynamic state lies within this inversion region, the speed of sound is drastically decreased and the same turbulent speed (here 20 m/s) leads to a highly compressible evolution of the turbulence. As it can be seen in Figure 9 for case MAH1, both LES simulations cannot capture the right evolution of the kinetic energy. One can first note that no oscillations of the kinetic energy are visible for the realistic resolution of 16^3 . This is coherent with the fact that these fluctuations relate to length scales smaller than 5 Kolmogorov length scales as suspected from the time evolution of the spectra in Figure 6. More importantly, even for the 32^3 resolution, LES fails to obtain the right slope of the curve of the kinetic energy in the case MAH1. Figure 9 also presents the same comparison for the case PG2. One can see that kinetic energy oscillations also disappear for the resolution comprising 16^3 elements. Yet, in this case LES results are much closer to DNS once the initial highly compressible phase of the simulation is over. After this transitional phase, LES seems to correctly predict the slope of the curve of the kinetic energy in contrast with what is observed for case MAH1.

4. Concluding remarks

A study of turbulence in BZT dense gas flows is performed using DNS. It is shown that for a large but realistic intensity ($\approx 10\%$ of a 200m/s average bulk velocity), the turbulence behaves in a highly compressible manner when the average thermodynamic state lies within the inversion region. As a consequence, similarities between the temporal evolutions of the kinetic energy are found between the case using the Martin & Hou Equation of State (EoS) and the perfect gas EoS when in addition of the Taylor Reynolds number, the turbulent Mach number is kept constant. Yet, in order to ensure such matching values, the turbulence intensity has to be increased in the perfect gas case to unrealistic levels (that might only be of interest for

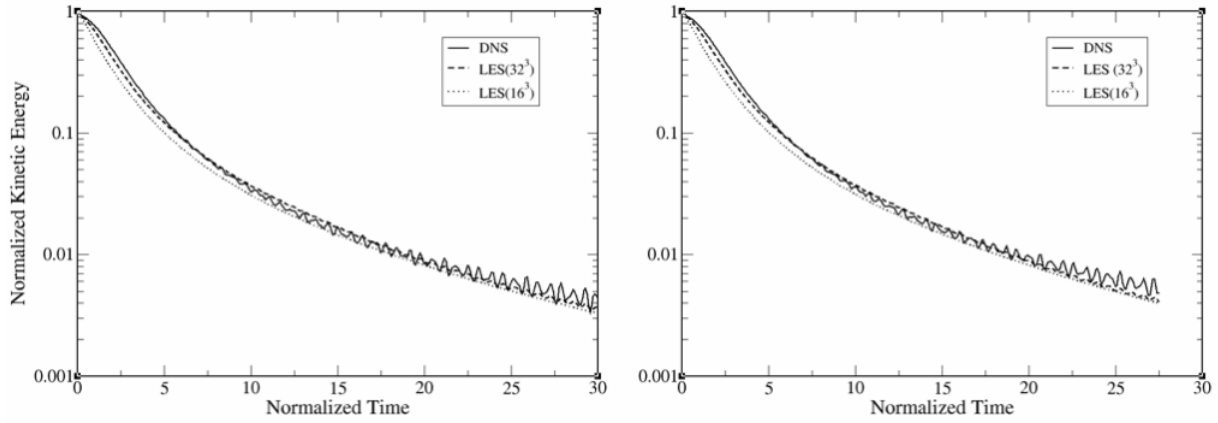


Figure 8. Evolution of the normalized kinetic energy with time with comparison between LES and DNS in the case MAH2(left) and PG1 (right).

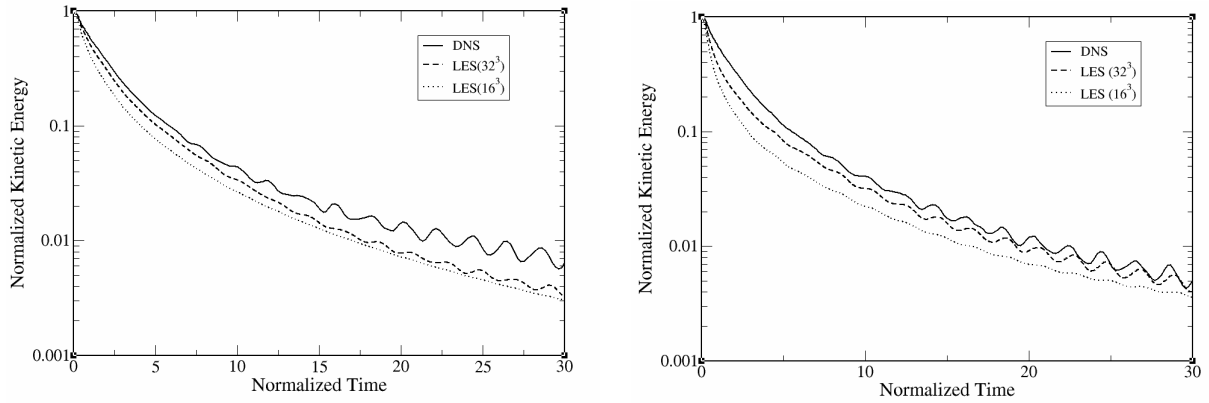


Figure 9. Evolution of the normalized kinetic energy with time with comparison between LES and DNS in the case MAH1(left) and PG2 (right).

interstellar flows). It is therefore expected that turbulent flows of dense gases will more easily present a characteristic compressible behavior that needs to be addressed through modeling if accurate Large Eddy Simulations (LES) of those flows are to be performed. In order to assess the capabilities of present LES subgrid-scale models, a-posteriori tests are performed using the dynamic Smagorinsky model. Coherently with the hypothesis it relies on, the model perfectly captures the evolution of the kinetic energy when the turbulent Mach number is low enough. When using the perfect gas EoS at a higher turbulent Mach number, the agreement is reasonable. Yet, for the dense gas case, when the average thermodynamic state lies within the inversion region, the model is not able to capture the correct evolution of the kinetic energy. Because of the renewed interest in this thermodynamic region, such turbulent flows will certainly be encountered in the future when using dense gases. Therefore, the results of this study call for a specific research effort assessing available subgrid-scale models and possibly developing advanced models for LES of turbulent dense gas flows (as for example the one proposed by Kosovic *et al* [17]). This research should also enable a deeper understanding of the phenomena at play in dense gas turbulence (such as for example the possible occurring of backscatter [18]).

Acknowledgement

The authors would like to thank Pr. Laadhari for insightful discussions on the theory of homogeneous isotropic turbulence. Simulation are carried out using HPC ressources at CINES under the project grant #c2016a7564.

References

- [1] P. A. Thompson, "A Fundamental Derivative in Gasdynamics," *Physics of Fluids*, vol. 14, no. 9, p. 1843, 1971.
- [2] A. Guardone and B. M. Argrow, "Nonclassical gasdynamic region of selected fluorocarbons," *Physics of Fluids*, vol. 17, no. 11, pp. 1–17, 2005.
- [3] S. Ferguson, T. Ho, B. M. Argrow, and G. Emanuel, "Theory for producing a single-phase rarefaction shock wave in a shock tube," *Journal of Fluid Mechanics*, vol. 445, pp. 37–54, 2001.
- [4] J. J. Martin and Y.-c. Hou, "Development of an Equation of State for Gases," *AIChE journal*, vol. 2, no. 4, pp. 142–151, 1955.
- [5] T. H. Chung, M. Ajlan, L. L. Lee, and K. E. Starling, "Generalized multiparameter correlation for nonpolar and polar fluid transport properties," *Industrial & Engineering Chemistry Research*, vol. 27, pp. 671–679, apr 1988.
- [6] T. Schönfeld and M. Rudgyard, "Steady and Unsteady Flow Simulations Using the Hybrid Flow Solver AVBP," *AIAA Journal*, vol. 37, pp. 1378–1385, nov 1999.
- [7] O. Colin and M. Rudgyard, "Development of High-Order TaylorGalerkin Schemes for LES," *Journal of Computational Physics*, vol. 162, pp. 338–371, aug 2000.
- [8] G. Staffelbach, L. Gicquel, G. Boudier, and T. Poinso, "Large Eddy Simulation of self excited azimuthal modes in annular combustors," *Proceedings of the Combustion Institute*, vol. 32, no. 2, pp. 2909–2916, 2009.
- [9] L. Gicquel, G. Staffelbach, and T. Poinso, "Large Eddy Simulations of gaseous flames in gas turbine combustion chambers," *Progress in Energy and Combustion Science*, vol. 38, pp. 782–817, dec 2012.
- [10] A. Giauque, L. Selle, L. Gicquel, T. Poinso, H. Buechner, P. Kaufmann, and W. Krebs, "System identification of a large-scale swirled partially premixed combustor using LES and measurements," *Journal of Turbulence*, vol. 6, p. N21, jan 2005.
- [11] P. Moin and K. Mahesh, "DIRECT NUMERICAL SIMULATION: A Tool in Turbulence Research," *Annual Review of Fluid Mechanics*, vol. 30, no. 1, pp. 539–578, 1998.
- [12] S. Kida and S. A. Orszag, "Energy and Spectral Dynamics in Decaying Compressible Turbulence," *Journal of Scientific Computing*, vol. 7, no. 1, 1992.
- [13] R. Samtaney, D. I. Pullin, and B. Kosović, "Direct numerical simulation of decaying compressible turbulence and shocklet statistics," *Physics of Fluids*, vol. 13, no. 5, pp. 1415–1430, 2001.
- [14] L. Sciacovelli and P. Cinnella, "Numerical Simulation of Dense Gas Compressible Homogeneous Isotropic Turbulence," in *15th European Turbulence Conference*, (Delft), 2015.
- [15] W. H. Reid and D. L. Harris, "Similarity Spectra in Isotropic Turbulence," *Physics of Fluids*, vol. 2, p. 139, nov 1959.
- [16] G. K. Batchelor, *The Theory of Homogeneous Turbulence*. Cambridge University Press, 1953.
- [17] B. Kosović, D. I. Pullin, and R. Samtaney, "Subgrid-scale modeling for large-eddy simulations of compressible turbulence," *Physics of Fluids*, vol. 14, no. 4, pp. 1511–1522, 2002.
- [18] J. O'Brien, J. Urzay, M. Ihme, P. Moin, and a. Saghafian, "Subgrid-scale backscatter in reacting and inert supersonic hydrogen-air turbulent mixing layers," *Journal of Fluid Mechanics*, vol. 743, pp. 554–584, 2014.